J Mater Sci: Mater Electron (2008) 19:1128–1134
DOI 10.1007/s10854-007-9485-0

Thermal conductivity and nanoindentation hardness of as-prepared and oxidized porous silicon layers

Zhenqian Fang · Ming Hu · Wei Zhang · Xurui Zhang · Haibo Yang

Received: 19 September 2007 / Accepted: 9 November 2007 / Published online: 5 December 2007
© Springer Science+Business Media, LLC 2007

Abstract Porous silicon (PS) offers promising possibilities to be applied as thermal insulating material in thermal effect microsystems for its thermal conductivity (TC) is up to two orders smaller than that of bulk silicon. In order to find a compromise between efficient thermal isolation and good mechanical stability of PS, thermal oxidation of PS is commonly used to tune the mechanical and thermal properties of PS. Both TC and the hardness of as-prepared and oxidized PS have been thoroughly investigated. TC and the hardness of as-prepared and oxidized PS were measured using micro-Raman scattering and nanoindentation, respectively. Experimental results revealed that TC and the hardness of as-prepared PS, exhibiting a strong dependence on the preparing conditions, decrease with increasing porosities. After oxidization at different temperatures, TC of oxidized PS decreases with increasing oxidation temperatures, whereas the hardness increases a lot. PS with a moderate porosity of 73.4% oxidized at 600 °C has a compromise between low TC [2.100 W/(m K)] and high hardness ($\sim$1.160 GPa). So this process finalizes this kind of oxidized PS to be used as a suitable thermal insulation substrate in thermal effect microsystems.

1 Introduction

Thermal effects play a quite fundamental role in the operation of many thermal effect microsystems [1, 2] such as resistive thin-film thermal temperature sensor, thermal flow sensor, IR detector, etc., which require a more reliable thermal insulation between their sensing elements and the silicon substrate in order to get efficient and accurate measurements. Minimization of thermal losses [3] is also one of the main requirements for the fabrication of these thermal effect microsystems, since the conductive heat flux from their sensing elements to the silicon substrate is becoming the dominant factor for heat losses with decreasing dimensions of these thermal effect microsensors.

Up to now, there are two main kinds of methods for ensuring better thermal isolation in thermal effect microdevices or microsystems [4]. Firstly, different materials with low thermal conductivity (TC), such as silicon dioxide, silicon nitride and polymer films, are used. Silicon dioxide has a low TC, which is about 1.5 W/(m K). To take advantage of this property, it is best that the oxide is thick. However, in a conventional thermal oxidation process at high temperature (>1,000 °C), only a few microns thick oxide is grown in 10 h, and it is not practical to produce layers thicker than 10 μm. As for silicon nitride, which is generally deposited by plasma enhanced chemical vapor deposition (PECVD), the standard thickness of thin nitride membranes is 0.2 μm [5]; the layer thickness of silicon nitride is limited due to poor thermal stability [6]. And its TC is much higher, which is about 30 W/(m K). Besides, the use of polymer films is not compatible with standard CMOS technology. Secondly, some freestanding monocrystalline silicon microstructures with high-thermal resistance can be realized by bulk-micromachining technology. These suspended microhotplates, membranes or cantilever beams have good thermal isolation with low effective thermal conduction decreasing the heat losses, but their mechanical properties are quite poor.

Z. Fang (✉) · M. Hu · W. Zhang · X. Zhang · H. Yang
School of Electronic & Information Engineering, Tianjin University, Tianjin 300072, China
e-mail: fangzhq@eyou.com

More recently, most studies dealing with TC of as-prepared porous silicon (PS) [1, 7–9] showed that TC of as-prepared PS is up to two orders smaller than that of bulk silicon [150 W/(m K)]. Wolf et al. [10] has measured TC of PS annealed at 1,000 °C, which is one or two orders smaller than the bulk value. Thick (up to 100 μm) as-prepared [11] and oxidized [12] PS layers displaying good mechanical properties can be easily obtained locally on a silicon wafer. At the same time, PS technique is compatible with standard CMOS technology. So PS can offer a good alternative for the thermal isolation in thermal effect microsystems. In order to improve the efficiency of measurement, a simple, reliable and effective TC measurement method in PS is quite necessary. Compared with other TC measurement techniques such as thermal sensors [13, 14], photoacoustic technique [15], optical pump-probe method [16], scanning thermal probe microscopy [17] and the lock-in thermography technique [10], the direct noncontact and nondestructive micro-Raman scattering spectroscopy method [8] is quite easy and accurate. Consequently, in this paper TC of as-prepared and oxidized PS as a function of the layer porosities and oxidation temperatures was measured by means of this recently proposed technique based on micro-Raman scattering spectroscopy.

Till now, only as-prepared PS has been characterized in terms of their mechanical properties [18], which decrease with the increment of porosities. However, the hardness of as-prepared PS is just measured by the static indentation tests which can not ensure precisely in micro/nano scale. To our knowledge, it should be noted that no mechanical data has been reported for oxidized PS. From our point of view, it is extremely necessary to perform a systematic study on finding the compromise between efficient thermal isolation and high mechanical stability of PS. So the hardness of as-prepared and oxidized PS with respect to contact depth was also measured by depth-sensing nano-indentation techniques.

2 Experimental details

2.1 Sample preparation

PS layers were formed by electrochemical anodisation of a (100)-oriented monocrystalline p^+ silicon wafer with 1–2×10^{-2} Ω cm resistivity and 380–420 μm thickness in a hydrofluoric acid/ethanol electrolyte and subsequently oxidized in a vacuum heat treatment system. The electrolyte consisted of 40 wt.% hydrofluoric acid and pure ethanol in a volume ratio of 1:1. The applied current density remained constant and the time of anodisation was 30 min. In order to obtain various PS porosities, three kinds of current densities ranging from 40 to 100 mA/cm^2 were selected. Another three samples prepared with the current density of 80 mA/cm^2 were oxidized for 1 h at different temperature of 300, 450, and 600 °C; the oxygen partial pressure was 5 Pa and oxygen flow rate was regulated to be 35 mL/min. The porosity of as-prepared PS was measured from gravimetric measurements [19]. The thickness of the samples was determined by a field emission scanning electron microscope (FESEM). Table 1 lists the experimental conditions used for as-prepared and oxidized PS. It is shown that it is easy to produce a suitable thickness ($\sim$50 μm) of as-prepared PS in a short etching time about 30 min. Figure 1 presents the surface FESEM micrographs of as-prepared PS. The etching direction is from top to bottom. According to IUPAC guidelines, PS has been classified depending on the size of micropore as micro-PS (<5 nm), meso-PS (5–50 nm) and macro-PS (>50 nm) [20]. It can be seen that the size of these micropores is about 5–40 nm and much <50 nm, therefore as-prepared PS belongs to meso-PS. With increasing current densities (increasing porosities), micropores become more enlarged and distribute more densely. Due to the incomplete surface etching of S1 with a low current density (40 mA/cm^2), there are some residual silicon scraps (white spots) as shown in Fig. 1a. However, the surfaces of S2 and S3 have been completely etched with increasing current densities, and there are no residual silicon scraps. The amount and size of micropores of S1 is less than that of S2 and S3. Besides, S3 has more big micro-pores. The surface FESEM images of another three as-prepared PS with the current density of 80 mA/cm^2 oxidized at 300, 450, and 600 °C are shown in Fig. 2. With increasing oxidation temperatures, the size of micropores and porosities of oxidized PS decrease greatly. Especially for S6 oxidized at 600 °C, more SiO_2 cladding layers were formed, so the pore-size and porosity is quite less than that of S4, S5 and as-prepared one. All these can be deduced that the mechanical stability of as-prepared PS will decrease with increasing porosities, whereas the mechanical stability of the same as-prepared ones after oxidized at different temperatures will improve a lot.

2.2 Micro-Raman scattering spectroscopy tests

TC of as-prepared and oxidized PS was measured by a direct noncontact and nondestructive method based on micro-Raman scattering spectroscopy [21]. A heating power source focused on the sample surface generates a thermal gradient through the material depending on its TC. TC of PS has a linear relationship between the heating power P and the local temperature rise T_j.

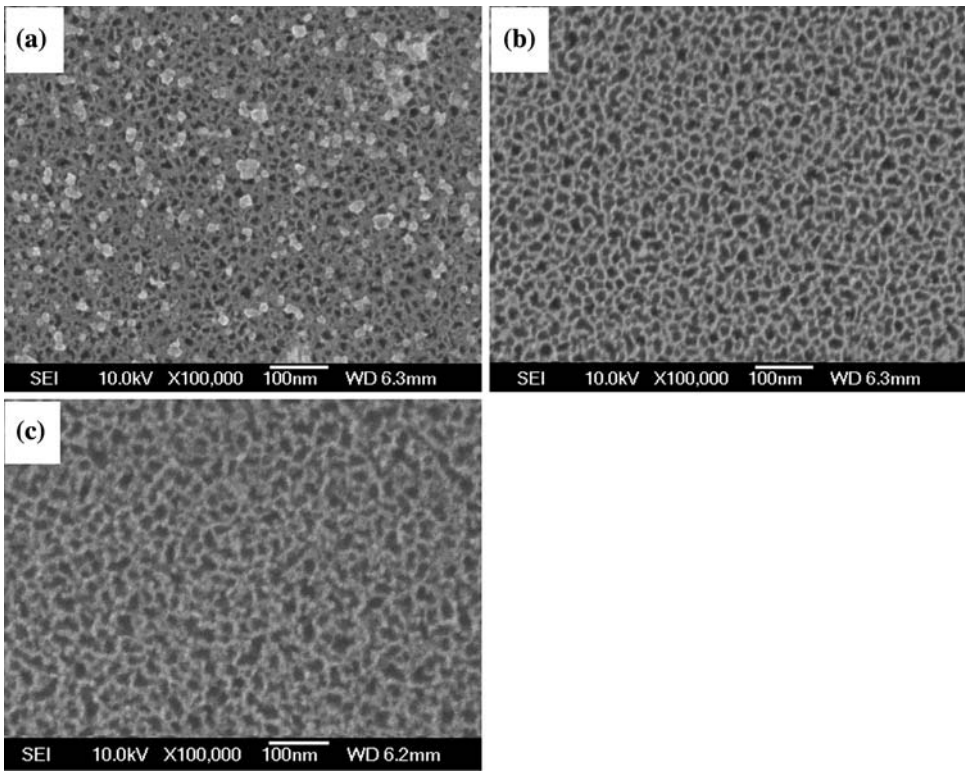

Fig. 1 FESEM images of as-prepared PS (**a**) S1; (**b**) S2; (**c**) S3

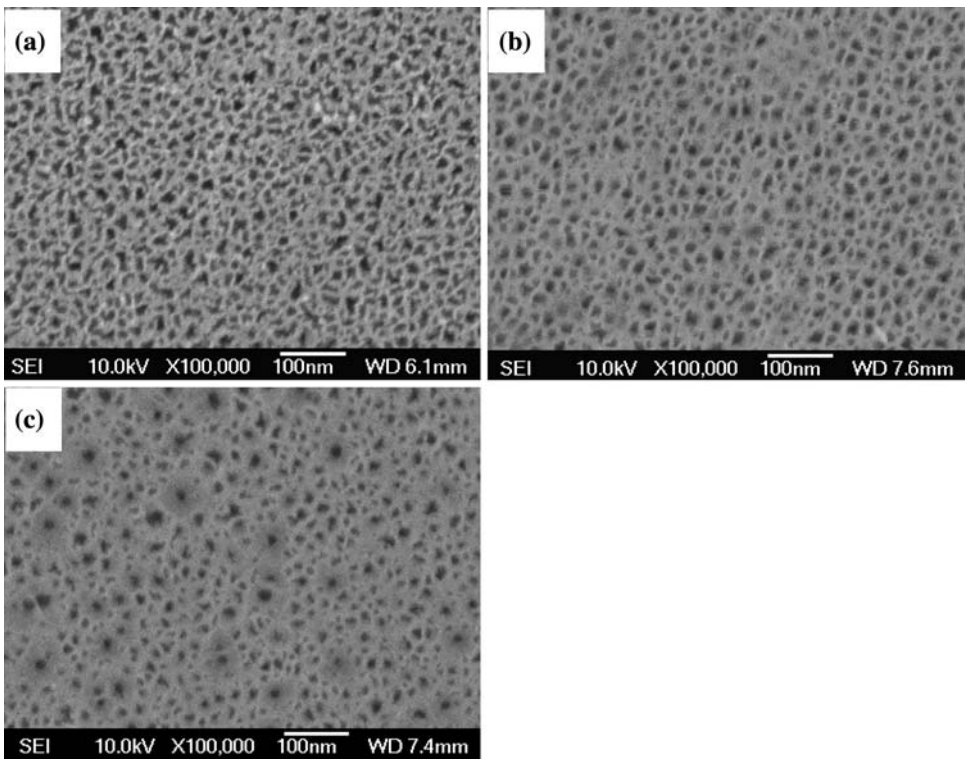

Fig. 2 FESEM images of oxidized PS (**a**) S4; (**b**) S5; (**c**) S6

$$\lambda = \frac{2P}{\pi a\left(T_{\mathrm{j}} - T_{\mathrm{b}}\right)}. \quad (1)$$

Here, T_{b} is the bulk temperature and α is the heating source diameter. Assuming a very shallow heat generation and PS layers absorbed about 100% of the incident light regarding their dark appearance, then heat losses in the air are thought to be negligible. The 50 μm layer of PS with a low TC is sufficient for neglecting the effect of silicon substrate. Thus, micro-Raman scattering spectroscopy is

Table 1 Parameters used for the preparation of as-prepared and oxidized PS

Sample	Current density (mA/cm^2)	Etching time (min)	Porosity (%)	Thickness (μm)	Oxidized temperature (°C)
S1	40	30	60.0	48	Room
S2	80	30	73.4	46	Room
S3	100	30	78.8	51	Room
S4	80	30			300
S5	80	30			450
S6	80	30			600

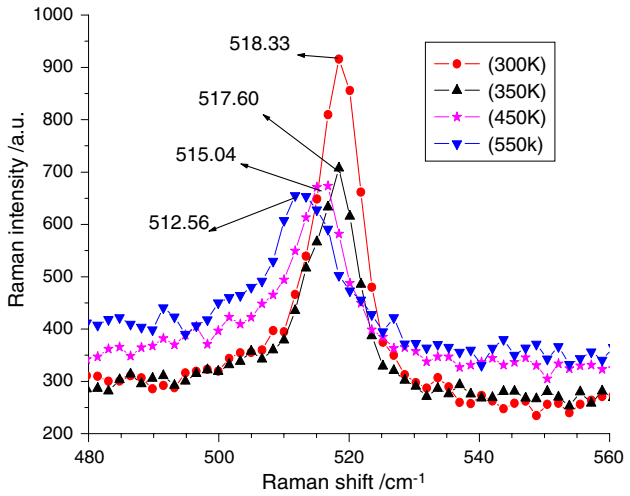

Fig. 3 Micro-Raman peak shifts of as-prepared PS under 1.2 mW

applicable. Firstly, PS was mounted on a temperature controlled element to heat to different temperatures with a low power P_l without inducing additional surface heating. From Raman peak shifts of PS under different temperatures, the calibration fitting curve of Raman peak shifts as a function of temperatures can be obtained. After that, using Raman peak shift of PS with a high power P_h under room temperature, the accurate local temperature rise T_j can be found in the exact calibration fitting curve. So knowing the heating power and the local temperature rise, TC of PS can be known in solving the Eq. 1.

In experiment, micro-Raman scattering spectroscopy was recorded by a RENISHAW RM2000 microscopic confocal Raman spectrometer with 20× objective lens over a wavenumber shift rage of 400–1,800 cm^{-1}. The spectral resolution was 1 cm^{-1}. The laser diameter was a fixed mean value, which was 5 μm. The output laser power is up to 4.7 mW. The excitation source of an Ar^+-ion laser with a wavelength of 514 nm was used to focus on PS samples. The bulk temperature T_b was 300 K. The Raman spectra were recorded at 300, 350, 450, and 550 K with a low laser power (25%) P_l of 1.2 mW. Then a high laser power (100%) P_h of 4.7 mW was used to get the local temperature rise T_j.

2.3 Nanoindentation tests

The hardness of as-prepared and oxidized PS was investigated by using a Nanoindenter XP system (MTS, American) with the continuous stiffness measurements (CSM) option. The CSM allows the hardness to be determined accurately as a function of contact depth with a single indentation. A sharp diamond Berkovich indenter, a three-side pyramid with a tip radius of ~40 nm, was used in all experiments. When CSM technique [22] is employed, the stiffness is measured continuously allowing the hardness to be calculated at every displacement point acquired during the nanoindentation tests. Detailed descriptions of the system, the CSM depth-sensing tests and analysis method used to determine the hardness have been published elsewhere [23]. The maximum indentation depth was 2,000 nm, and therefore quite less than 10% of the total thickness of the specimen layer, which ensured that the mechanical properties of the specimen layer were being measured without major influence from the underlying silicon substrate [24]. The hardness of each sample was averaged with respect to contact depth.

3 Results and discussion

3.1 Thermal conductivity and hardness of as-prepared PS layers

Figure 3 illustrates the micro-Raman peak shifts of as-prepared PS under a low laser power P_l of 1.2 mW. Figure 4 is the calibration fitting curve of the micro-Raman peak shifts versus temperatures for as-prepared PS.

Table 2 shows the micro-Raman peak shifts of as-prepared PS samples S1, S2, and S3 recorded under a high laser power P_h of 4.7 mW, the resultant local temperature rise deduced from Fig. 4 and TC calculated from Eq. 1.

As one can see in Table 2, TC of as-prepared PS decreases with increasing porosities. Sample S1 with a porosity of 60.0% generates smallest local temperature rise of 482.45 K under a high laser power P_h of 4.7 mW, and its TC is 3.282 W/(m K). Sample S2 with a moderate

Table 2 Micro-Raman peak shifts, local temperature rise and TC of as-prepared samples S1, S2 and S3

Sample	Porosity (%)	Micro-Raman peak shift (cm^{-1})	Local temperature rise (K)	TC [W/(m K)]
S1	60.0	514.23 ± 0.5	482.45	3.282
S2	73.4	507.47 ± 0.5	768.61	1.278
S3	78.8	505.78 ± 0.5	840.06	1.109

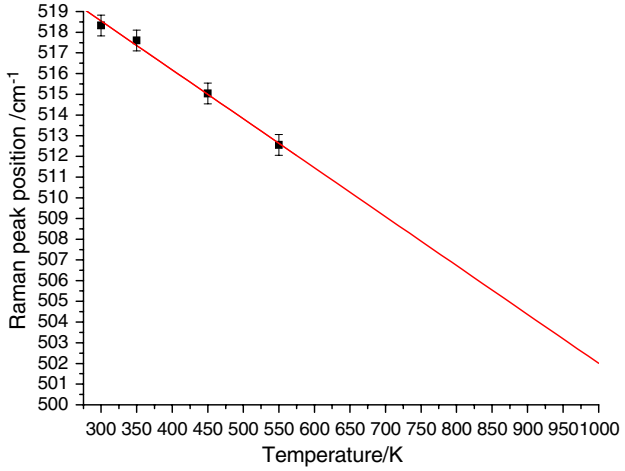

Fig. 4 Calibration fitting curve of as-prepared PS

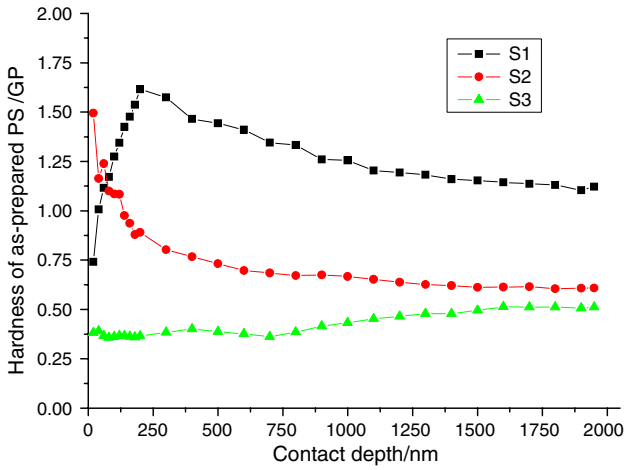

Fig. 5 Curves of hardness with respect to contact depth for as-prepared PS

porosity of 73.4% has a local temperature rise of 768.61 K, and its TC decreases to be 1.278 W/(m K). As to sample S3, it has a porosity of 78.8%, has much greater local temperature rise of 840.06 K and quite smaller TC of 1.109 W/(m K). At the same time, these measured TC-values of as-prepared PS are qualitatively to be about two orders lower than that of monocrystalline silicon substrate. Taking into account the main random error that is the uncertainty on the Raman peak position estimated to be ±0.5 cm^{-1}, the relative error of the local temperature rise deduced from Fig. 4 is about ±20 K. So the relative errors on the measured TC of S1, S2, and S3 in Table 2 are estimated to be 12.2, 3.9, and 3.6%, respectively.

Figure 5 shows the variation of hardness as a function of contact depth for as-prepared PS. Due to the finite radius of the real tip diamond indenter [23, 25], the hardness curve shows a maximum value at shallow contact depth. After that, the hardness gradually decreases for higher contact depth to a clear plateau region. The evaluation of the hardness in experiments is based on the average value in the plateau region. The size of micropores in Fig. 1a is quite less than the radius of the diamond Berkovich indenter (40 nm), so the hardness curve of S1 shows a peak. The size of micropores in Fig. 1b is near to 40 nm, and then the hardness decreases strongly with increasing contact depth. While S3 has more big micropores (∼40 nm) as shown in Fig. 1c, the hardness is rather constant. It is also found that the hardness curve of S1 is on the top, then the curves of S2 and S3 in turn. The hardness of as-prepared S1 sample at a contact depth corresponding to ∼1,000 nm is ∼1.255 GPa, while that of S2 and S3 decreases to ∼0.667 and ∼0.432 GPa, respectively. These data are accordance with the corresponding analysis of the mechanical properties of as-prepared PS from FESEM images in Fig. 1. The size and density of micropores of S1 is less than that of S2 and S3, so the more residually interconnected silicon can strengthen the structure. The average hardness of as-prepared PS decreases with increasing porosities. Due to the microstructure changes of as-prepared PS with the augment of porosities, the decrease

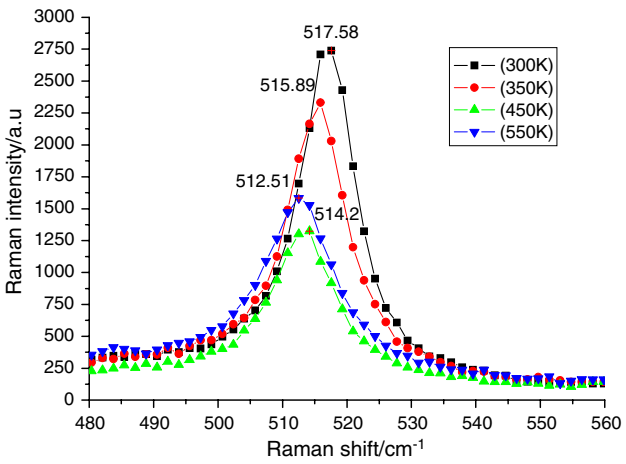

Fig. 6 Micro-Raman peak shifts of oxidized PS under 1.2 mW

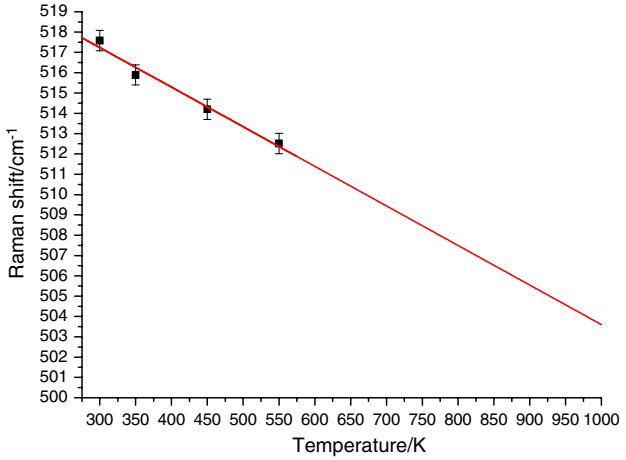

Fig. 7 Calibration fitting curve of oxidized PS

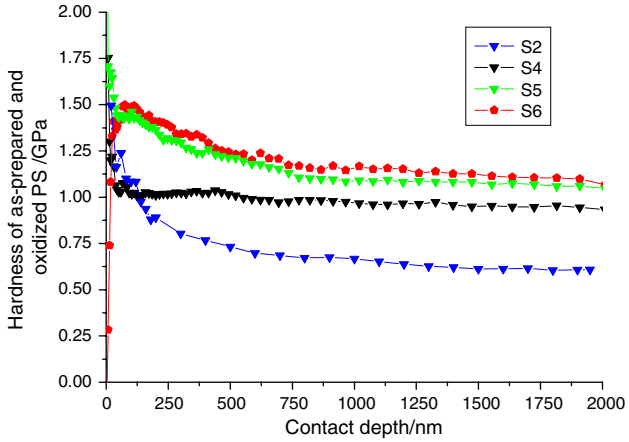

Fig. 8 Comparative curves of hardness with respect to contact depth for as-prepared and oxidized PS

in hardness is attributed to the formation of interconnected incompact sponge microstructure [26] of silicon columns and pores or isolated nanocrystallites in as-prepared PS.

So from Table 2 and Fig. 5, considering a compromise between low TC and high mechanical stability, as-prepared PS with a moderate porosity of 73.4% has a compromise between TC value [1.278 W/(m K)] and the hardness (~0.667 GPa), and it can be used as thermal insulating substrate in thermal effect microsystems.

3.2 Thermal conductivity and hardness of oxidized PS layers

TC of as-prepared PS decreases with increasing porosities, whereas the mechanical stability also decreases. Normally, suitable thermal treatments are recommended either to passivate as-prepared PS from chemical point of view or render them mechanically more stable. In order to study the effects of thermal treatments on TC and hardness of PS, another three as-prepared PS samples etched with the current density of 80 mA/cm^2 were oxidized at 300, 450, and 600 °C. Figure 6 shows the micro-Raman peak shifts of oxidized PS under a low laser power P_l of 1.2 mW. And the calibration fitting curve of oxidized PS is shown in Fig. 7.

From Fig. 6, one will easily find that the micro-Raman peak shifts of oxidized PS are smaller than that of as-prepared PS shown in Fig. 3. This denotes that much higher heat conductance of oxidized PS will engender lower surface temperature rise than that of as-prepared PS. Table 3 shows the micro-Raman peak shifts, local temperature rise deduced from Fig. 7 and the calculated TC of oxidized samples S4, S5, and S6. TC of S4, S5, and S6 is 3.846, 2.466, and 2.100 W/(m K), respectively. More SiO_2 cladding layers are formed at high oxidation temperature, so TC-values of oxidized samples decrease with the increment of oxidation temperatures. TC increases a little in the case of oxidized PS compared to as-prepared PS S2 [1.278 W/(m K)]. As shown in Fig. 1b and 2a–c, both the size of micropores and porosities of oxidized PS samples decrease after oxidized at different temperatures. So this TC difference can be explained by the larger structure size of oxidized PS and thus weaker size effect based on the phonon diffusion model [27] of the effective medium theory. And it is coincidence with TC analysis of sintered PS [10]. Considering the main random error that is the uncertainty on the Raman peak position estimated to be ±0.5 cm^{-1}, the relative error of the local temperature rise deduced from Fig. 7 is about ±25 K. So the relative errors on the measured TC of S4, S5, and S6 in Table 3 are estimated to be 15.6, 10.1, and 9.5%, respectively.

Figure 8 shows the comparative curves of hardness as a function of contact depth for as-prepared and oxidized PS. Only the size of micropores in Fig. 2c is quite less than the radius of the diamond Berkovich indenter (40 nm), so the hardness curve of S6 has a peak at shallow contact depth and shows the same behavior like S1 in Fig. 5. While the size of micropores in Fig. 2a, b is near to 40 nm, the

Table 3 Micro-Raman peak shifts, local temperature rise and TC of oxidized samples S4, S5 and S6

Sample	Oxidized temperature (°C)	Micro-Raman peak shift (cm^{-1})	Local temperature rise (K)	TC [W/(m K)]
S4	300	514.20 ± 0.5	455.61	3.846
S5	450	512.51 ± 0.5	542.66	2.466
S6	600	511.68 ± 0.5	585.09	2.100

corresponding hardness curves behave like S2 in Fig. 5, which decrease strongly with increasing contact depth. It can be seen that the hardness of oxidized PS improves greatly with increasing oxidation temperatures and is much bigger than that of as-prepared one. Compared with the hardness of S2 ($\sim$0.667 GPa) , the hardness of S4 (oxidized at 300 °C), S5 (oxidized at 450 °C) and S6 (oxidized at 600 °C) at a contact depth corresponding to $\sim$1,000 nm is improved to be $\sim$0.963, $\sim$1.084, and $\sim$1.160 GPa, respectively. The increase of hardness is due to the changes of porosities and the formation of silicon dioxide in thermal oxidation at different temperatures. After thermal oxidation, as-prepared PS is partially oxidized to form SiO_2 cladding layers encapsulating on the inner surface of the incompact sponge PS to decrease the porosity and strength the interconnected microstructure.

Therefore, oxidized PS S6 not only can have a low TC [2.100 W/(m K)], but also can guarantee a much better structural and mechanical stability ($\sim$1.160 GPa). Even if its TC is a little greater than that of as-prepared PS [1.278 W/(m K)] in Table 2, the mechanical stability of this sample is improved greatly. As-prepared PS with a moderate porosity of 73.4% oxidized at 600 °C can be used as a suitable thermal insulation substrate in thermal effect microsystems for the compromise between low TC and high mechanical stability.

4 Summary

In this work, TC of as-prepared and oxidized PS was measured by using a direct noncontact and nondestructive technique based on micro-Raman scattering spectroscopy. At the same time, the hardness of as-prepared and oxidized PS with respect to contact depth was also investigated by depth-sensing nanoindentation techniques with the continuous stiffness measurements (CSM) option. TC and the hardness of as-prepared PS decrease with increasing porosities. TC and the hardness of as-prepared PS with porosities of 60.0, 73.4, and 78.8% are [3.282 W/(m K), $\sim$1.255 GPa], [1.278 W/(m K), $\sim$0.667 GPa] and [1.109 W/(m K), $\sim$0.432 GPa], respectively. As-prepared PS with a moderate porosity of 73.4% has a compromise between TC-value [1.278 W/(m K)] and the hardness ($\sim$0.667 GPa). TC of these kinds of as-prepared samples oxidized at different temperatures decreases with increasing oxidation temperatures, whereas the hardness increases a lot. TC of as-prepared samples oxidized at 300, 450, and 600 °C is 3.846, 2.466, and 2.100 W/(m K), respectively. Although TC of oxidized PS samples is a little greater than that of as-prepared one, they are quite near to each other. Besides, the hardness is improved from $\sim$0.667 to be $\sim$0.963, $\sim$1.084, and $\sim$1.160 GPa, respectively. Consequently, considering the compromise between an efficient thermal insulation and high mechanical stability, as-prepared PS with a moderate porosity of 73.4% oxidized at 600 °C can be used as a suitable thermal insulation substrate in thermal effect microsystems.

Acknowledgements This work was supported by National Natural Science Foundation of China No. 60371030 and Natural Science Foundation of Tianjin of China No. 023603811. The authors would like especially to thank Professor Jianyuan Yu at Tsinghua University and Professor Dejun Li at Tianjin Normal University for their constant supports, suggestions and helpful discussion in micro-Raman scattering spectroscopy and nanoindentation measurements.

References

1. G. Gesele, J. Linsmeier, V. Drach, J. Fricke, R. Arens-fischer, J. Phys. D: Appl. Phys. **30**, 2911 (1997)
2. S. Perichon, V. Lysenko, P. Roussel, B. Remaki, B. Champagnon, D. Barbier, P. Pinard, Sens. Actuators A **85**, 335 (2000)
3. C. Tsamis, A.G. Nassiopoulou, A. Tserepi, Sens. Actuators B **95**, 78 (2003)
4. V. Lysenko, S. Perichon, B. Remaki, D. Barbier, Sens. Actuators A **99**, 13 (2002)
5. R. Triantafyllopoulou, S. Chatzandroulis, C. Tsamis, A. Tserepi, Microelectronic Eng. **83**, 1189 (2006)
6. S.J. Patil, D.S. Bodas, A.S. Ethiraj, R.C. Purandare, G.J. Phatak, S.K. Kulkarni, S.A. Gangal, Vacuum **65**, 91 (2002)
7. G. Benedetto, L. Boarino, R. Spagnolo, Appl. Phys. A. **64**, 155 (1997)
8. V. Lysenko, S. Perichon, B. Remaki, D. Barbier, B. Champagnon, J. Appl. Phys. **86**, 6841 (1999)
9. Q. Shen, T. Toyoda, Rev. Sci. Instrum. **74**, 601 (2003)
10. A. Wolf, R. Brendel, Thin Solid Films **513**, 385 (2006)
11. T. Pichonat, B. Gauthier-Manuel, J. Membr. Sci. **280**, 494 (2006)
12. P.H. Roussel, V. Lysenko, B. Remaki, G. Delhomme, A. Dittmar, D. Barbier, Sens. Actuators. **74**, 100 (1999)
13. M. Okuda, S. Ohkubo, Thin Solid Films. **213**, 176 (1992)
14. F.R. Brotzen, P.J. Loos, D. Pbrady, Thin Solid Films **207**, 197 (1992)
15. E. Monticone, L. Boarino, G. Lerondel, R. Steni, G. Amato, V. Lacquaniti, Appl. Sur. Sci. **142**, 267 (1999)
16. U. Bernini, S. Lettieri, P. Maddalena, R. Vitiello, G. Difrancia, J. Phys. Condens. Matter. **13**, 1141 (2001)
17. V. Lysenko, S. Volz, Phys. Stat. Sol. A. **182**, R6–R7 (2000)
18. S.P. Duttagupta, P.M. Fauchet, in*Properties of Porous Silicon*, ed. by L.T. Canham (INSPEC, London, UK, 1997), p. 132
19. G. Bhagavannarayana, S.N. Sharma, R.K. Sharma, S.T. Lakshmikumar, Mater. Chem. Phys. **97**, 442 (2006)
20. L.T. Canham, Appl. Phys. Lett. **57**, 1046 (1990)
21. S. Perichon, V. Lysenko, B. Remaki, B. Champagnon, D. Barbier, J. Appl. Phys. **86**, 4700 (1999)
22. W.C. Oliver, G.M. Pharr, J. Mater. Res. **7**, 1564 (1992)
23. S. Logothetidis, C. Charitidis, Thin Solid Films **353**, 208 (1999)
24. J. Wang, W.Z. Li, H.D. Li, B. Shi, J.B. Luo, Thin Solid Films **366**, 117 (2000)
25. S. Logothetidis, C. Charitidis, P. Patsalas, Diam. Rel. Mater. **11**, 1095 (2002)
26. L. Clement, S. Lust, M. Mamor, J. Rappich, T. Dittrich, Phys. Stat. Sol. A **202**, 1390 (2005)
27. V. Lysenko, P. Roussel, B. Remaki, G. Delhomme, A. Dittmar, D. Barbier, J. Porous Mater. **7**, 177 (2000)